Available online at www.sciencedirect.com
SCIENCE DIRECT®
Composites: Part B 35 (2004) 251–261
composites Part B: engineering
www.elsevier.com/locate/compositesb

Stress and failure analysis of wood composites: a new model

D.M. Moses[a], H.G.L. Prion[b,*]

[a]Equilibrium Consulting Inc., 1585 W. 4th Avenue, Vancouver, BC V6J 1L 6 Canada
[b]Department of Civil Engineering, The University of British Columbia, 2324 Main Mall, Vancouver, BC V6T 1Z4 Canada

Abstract

Structural wood composites are frequently used in building construction for beams and columns. While the technology for the production of these composites is highly advanced, modeling techniques to predict material behaviour in building applications are severely lacking. This paper proposes a material model that is based on orthotropic elasticity, anisotropic plasticity for non-linear behaviour in compression and the Weibull weakest link theory to predict brittle failure. This three-dimensional model is implemented using finite element analysis for two sample cases: the notched shear block specimen and a single-bolt connection specimen. Model output is compared against laboratory test results and provides detailed information on load–displacement, ultimate strength and mode of failure.

Keywords: A. Wood; B. Anisotropy; C. Finite element analysis; C. Statistical methods

1. Introduction

It is only recently that wood composites have been used as full size beams and columns in building construction. These composite structural elements have been welcomed by the construction industry for a number of reasons including: (1) reduced strength variability compared to solid lumber; (2) dimensional stability and (3) reduced reliance on old growth trees by using smaller diameter trees from species that grow faster. While the technology to produce wood composites has advanced significantly, predicting the behaviour of the material has not. To successfully introduce these new materials into the mainstream construction market, the industry needs reliable and detailed modeling techniques to predict the influence of species, strand size and other variables on the engineering properties of wood composites. With proper modeling, further improvements on production efficiency and material properties can be gained.

Material modeling of wood and the simulation of panel lay-ups are critical starting points to controlling the strength and stiffness of wood composites and understanding the performance of mechanical connections. In this study, a new material model is proposed to describe the mechanical behaviour of wood and wood composites. This model is used to predict behaviour in two applications: a notched shear block test specimen and a single-bolt connection. Both applications are verified with experimental data based on custom-fabricated wood composite panels, similar in make-up to commercially produced laminated strand lumber (LSL).

2. Laminated strand lumber

LSL is a panel composite made from wood strands approximately 30 cm long, 2.5 cm wide and less than 1 mm thick. Panels are typically fabricated from aspen (Populus tremuloides) or yellow-poplar (Liriodendron tulipifera) strands by orienting resin-sprayed strands into large mats followed by the application of steam and pressure. Using this process, panels up to 75 mm thick can be formed and then cut into beams or columns. Strand orientation in the plane of the panel can be controlled to increase axial and bending stiffness and strength. Although most strands in commercial LSL are oriented in one direction, limitations in the manufacturing process result in a significant percentage of cross-aligned strands. This results in reduced stiffness and strength in the direction parallel to the strands and increased stiffness and strength in the orthogonal in-plane direction (in the plane of the strands). Panel properties are thus highly dependent on strand orientation and stacking sequence [1].

The aspen panels for the current study were hand-laid to better control the orientation of the strands and to fabricate

* Corresponding author. Tel.: +1-604-822-3864; fax: +1-604-822-6901.
E-mail address: prion@civil.ubc.ca (H.G.L. Prion).

1359-8368/$ - see front matter © 2003 Elsevier Ltd. All rights reserved.
doi:10.1016/j.compositesb.2003.10.002

Nomenclature

d	bolt or dowel diameter (mm)
E_i	modulus of elasticity (MPa)
E_{tang}, E_T	tangent modulus (MPa)
e	end distance (mm)
F_i, F_{ij}	strength tensors of second and fourth rank (MPa^{-1}, MPa^{-2})
F_v	probability of failure
G_{ij}	shear modulus (MPa)
I	integral function
$[J]$	Jacobian matrix
K	effective yield stress (MPa)
k	shape parameter for Weibull distribution
l	length of bolt or thickness of wood member (mm)
M_{ij}	anisotropic strength parameters in tensorial form
m	scale parameter for Weibull distribution (MPa)
p	probability of failure
V_i	specimen volume
V^*	reference volume (m^3)
X, Y, Z	principal axes of orthotropy
x, y, z	material and global co-ordinate system
σ_{+i}, σ_{-i}	yield stress in tension or compression (MPa)
σ^*	reference stress for Weibull distribution (MPa)
σ_{ij}	shear stress in material coordinate system (MPa)

Abbreviations

A, B, C, D, E	panel lay-up types
AN	specimens cut at 45° to main strand axis
LSL	laminated strand lumber
Pa	specimens cut parallel to main strand axis
Pe	specimens cut perpendicular to main strand axis
R	randomly oriented layers

panels with stacking orientations that are not used in commercial production at the moment. The average panel density was tested to be at 690 kg/m^3. The following stacking sequences were used for this investigation (Fig. 1): (A) fully oriented (100%); (B) fully random (0%); (C) three equally thick layers with surfaces oriented and the core random (66%); (D) three layers with surfaces random and the core oriented (33%) and (E) eight oriented layers aligned at angles 0 and $\pm 45°$ (50%). The numbers in parentheses refer to the percentage of strands oriented along the primary strength axis.

Test specimens were cut from these panels for single-bolt connections and for standard tension, compression and shear tests to determine orthotropic properties.

3. Material properties: test methods

Basic uniaxial material properties were required to develop the constitutive relations for LSL for use in the finite element model. Extensive details can be found in Ref. [2]; however, a summary is provided here. The specimens were stored for 2 months in controlled conditions of 65% relative humidity and 20 °C. Moisture content at testing was approximately 9% on average. In all tests, careful attention was paid to the conditions at the onset of failure and to the mode of failure. Tension and compression properties were tested in the three material directions X, Y and Z shown in Fig. 1. Shear properties were tested in the XY, YZ and XZ planes. Tension behaviour in the plane of the panel was determined using modified ASTM D1037 [3] specimens. Two lengths were tested in each direction in the plane of the panel to determine the size effect relationship. Elastic modulus was also determined. The ultimate tensile strength perpendicular to the panel surface was determined using ASTM D1037 internal bond specimens. Two specimen thicknesses were tested to determine the size effect. Elastic modulus was not measured using these specimens.

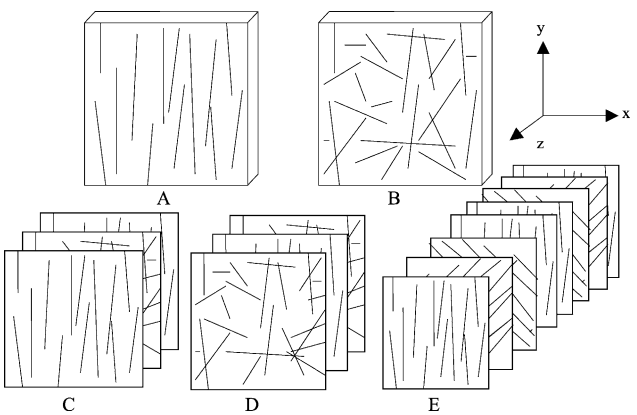

Fig. 1. LSL panel stacking sequence. 'A' fully oriented. 'B' randomly oriented. 'C' 0°/R/0°, 'D' R/0°/R. 'E' 0°/+45°/−45°/0/0/−45°/+45°/0. (R indicates random layer).

Compression in the plane of the panel was measured using to ASTM D143 [4] specimens in the X and Y-directions. Compression in the Z-direction was measured using a $38 \times 38 \times 38$ mm^3 block specimen. In compression, non-linear load–displacement behaviour was measured to determine elastic modulus, tangent modulus and ultimate stress.

Shear behaviour was measured according to ASTM D143 [4]. Two specimen sizes were tested in each orientation to determine if the size effect could be measured.

The six Poisson's ratios were measured for panel types 'A' and 'B' using three non-standard compression specimens. The two specimens loaded in the plane of the panel (X and Y-directions) had dimensions $25 \times 25 \times 100$ mm^3. Perpendicular to the plane of the panel (Z-direction), the test specimens had dimensions $25 \times 25 \times 38$ mm^3. Ten replicates were tested for each type of specimen. The Poisson's ratios were determined from data prior to

the onset of non-linear stress–strain behaviour. Four steel pads were mounted to the sides of each specimen with a 25 mm gauge length to accommodate a bi-axial extensometer. The Poisson's ratio was determined from the ratio of transverse to axial strains for each specimen.

4. Material properties: results

The observed test behaviour was typical for wood and wood composites: tension stress–strain behaviour was found to be linear elastic to failure and different in the three primary orthotropic directions; ultimate tension strengths in the three directions for different size specimens were well-fitted with the Weibull probability distribution (commonly used to represent the distribution of strength of wood); compression behaviour, shown in Fig. 2 for panel type A, was found to be elastic until a point, upon which behaviour was ductile and nearly bi-linear in each of the three primary material directions; shear behaviour, shown in Fig. 3 for panel type A, was linear elastic followed by brittle failure; ultimate shear strengths in the three principal shear planes for different size specimens were well-fitted with the Weibull distribution. Fitted values of properties are given in Tables 1a and 1b.

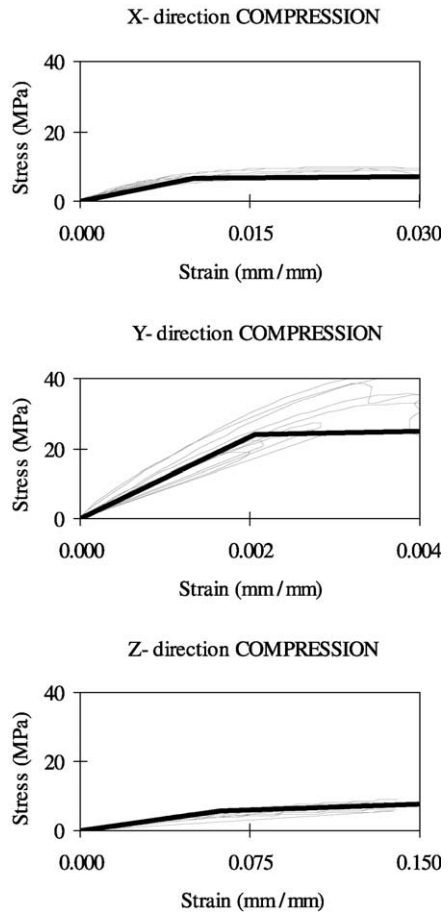

Fig. 2. Stress–strain experimental curves for compression behaviour in type 'A' LSL. Anisotropic plasticity curves shown in dark.

5. Material modeling

Three-dimensional finite element models have been used to predict delamination failure in fibre-reinforced plastic composites due to out-of-plane normal and shear stresses [5,6]. Currently, there is no generally accepted theory for the prediction of elastic and plastic stiffness and strength properties in wood. Based on the test results, as observed in this study, it is evident that the new model for wood and wood composites should incorporate orthotropic elasticity, anisotropic plasticity for the non-linear properties of wood in compression, and the size effect to predict ultimate strength for brittle modes of failure. The material model was created in ANSYS [7] using the built-in orthotropic elasticity and the anisotropic plasticity models and a user-programmable routine to predict brittle failure.

The anisotropic plasticity material model has been shown to effectively predict the behaviour of non-wood composites in two-dimensional finite element models [8]. This model accounts for permanent deformation and energy dissipation in three orthogonal planes. It is based upon the yield criterion for orthotropic materials and can accommodate differences in compression and tension yield stresses in each direction [9,10]. The model uses work hardening [11] and an associative flow rule. Details on this model can be found in any of the above references. A sample bi-linear stress–strain curve for the anisotropic plasticity model is shown in Fig. 4: the yield stress and tangent modulus for one material direction are shown. The two other normal stress–strain curves and three shear stress–strain curves are also required for this model resulting in a total of 18 constants.

Two criteria must be satisfied when using this model. To satisfy the requirement for plastic incompressibility, the yield stresses σ_{+i} and σ_{-i} in tension and compression, respectively, are inter-related

$$\frac{\sigma_{+x}-\sigma_{-x}}{\sigma_{+x}\sigma_{-x}}+\frac{\sigma_{+y}-\sigma_{-y}}{\sigma_{+y}\sigma_{-y}}+\frac{\sigma_{+z}-\sigma_{-z}}{\sigma_{+z}\sigma_{-z}}=0 \tag{1}$$

To maintain a closed yield surface

$$M_{11}^2+M_{22}^2+M_{22}^2-2(M_{11}M_{22}+M_{22}M_{33}+M_{11}M_{33})<0 \tag{2}$$

where

$$M_{ii}=\frac{K}{\sigma_{+i}\sigma_{-i}}(i=1,2,3) \tag{3}$$

and

$$K=\sigma_{+x}\sigma_{-x} \tag{4}$$

Eq. (2) must be satisfied at all levels of strain since the yield stresses will change as work hardening proceeds.

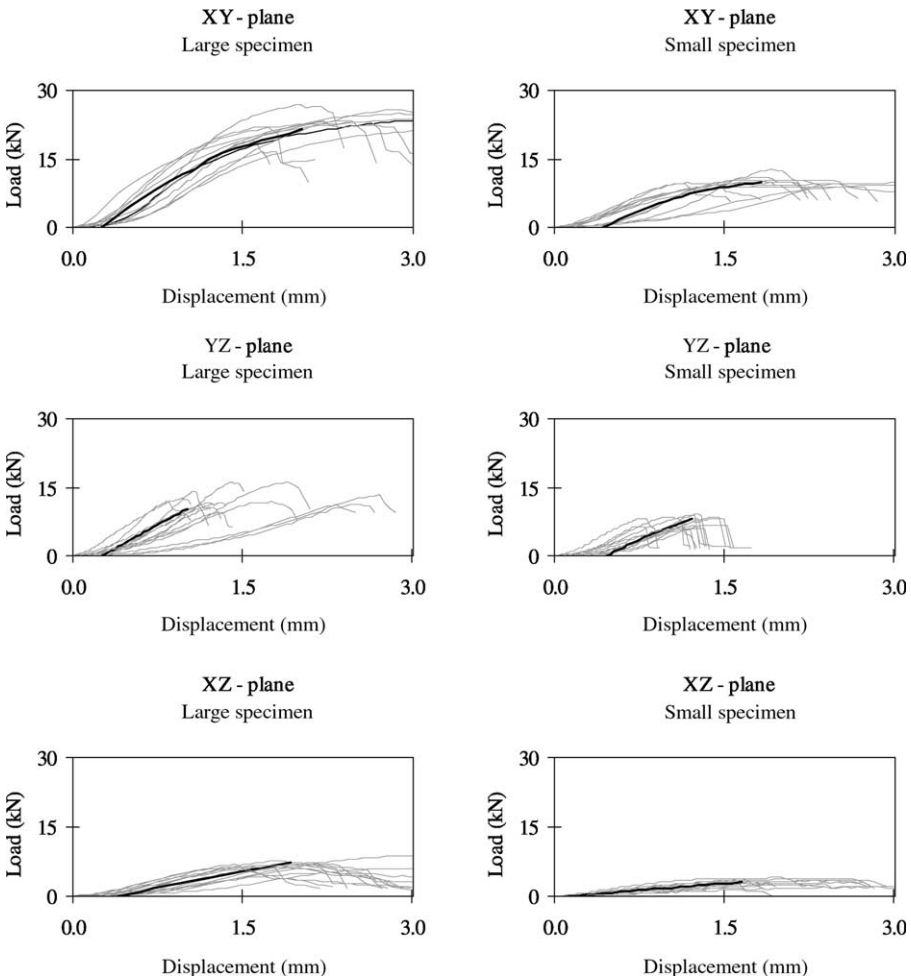

Fig. 3. Load–displacement curves for shear blocks in type 'A' LSL. Predicted curves shown in dark.

Table 1(a)
Material properties for uniaxial behaviour of LSL with anisotropic plasticity model

	Type A fully oriented panels (MPa)	Type B randomly oriented panels (MPa)
E_x	655	5516
E_y	11,721	5516
E_z	90	103
E_{Tx}	31	57
E_{Ty}	345	57
E_{Tz}	25	23
σ_{-x}	6.6	16
σ_{-y}	24	16
σ_{-z}	5.6	9.0

Tension values	Yield 'A' σ_{+i} (MPa)	Ultimate 'A' σ_i^* ($V = 16.4$, $p = 0.5$)	Yield 'B' σ_{+i} (MPa)	Ultimate 'B' σ_i^* ($V = 16.4$, $p = 0.5$)
X	6.6	4.8	16	22.7
Y	24	52.7	16	22.7
Z	5.6	1.3	9.0	1.2

Poisson's ratios not shown.

The restrictions imposed by Eqs. (1) and (2) make it difficult to fit experimental results to this plasticity model. This is particularly true for highly orthotropic materials such as LSL. To simplify the problem, the yield stresses in tension

Table 1(b)
Material properties for shear behaviour of LSL with anisotropic plasticity model

	Type A fully oriented panels (MPa)	Type B randomly oriented panels (MPa)
G_{xy}	1379	2068
G_{yz}	421	345
G_{xz}	179	345
G_{Txy}	3.4	3.4
G_{Tyz}	3.4	3.4
G_{Txz}	3.4	3.4
$\sigma_{\pm xy}$	34	55
$\sigma_{\pm yz}$	55	55
$\sigma_{\pm xz}$	55	55

	Ultimate 'A' σ_i^* ($V = 16.4$, $p = 0.5$)	Ultimate 'B' σ_i^* ($V = 16.4$, $p = 0.5$)
XY	20.4	23.4
YZ	8.3	8.1
XZ	5.4	8.1

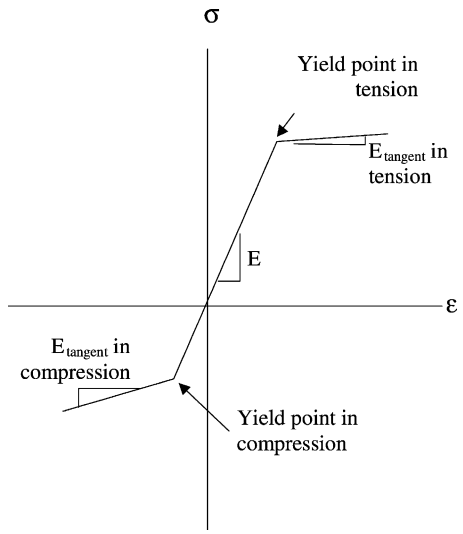

Fig. 4. Bi-linear stress–strain curve for normal stress in anisotropic plasticity model.

and compression were set equal to each other for each direction (i.e. $\sigma_{+x} = \sigma_{-x}$, $\sigma_{+y} = \sigma_{-y}$, $\sigma_{+z} = \sigma_{-z}$). However, the tension and shear yield stresses were set artificially high to avoid yield conditions; the failure analysis was used to detect brittle failure prior to the onset of fictitious yielding. A spreadsheet was developed using an optimization algorithm to satisfy these conditions up to 20% plastic strain.

Sample stress–strain curves for LSL are shown in Fig. 2. Model constants are listed in Tables 1a and 1b.

6. Failure prediction

The material model is crucial for determining the state of stress in a member under any given load. The failure model, on the other hand, must be capable of analysing the state of stress to determine whether or not brittle failure has occurred. Several criteria have been developed that are applicable to wood and orthotropic materials, although most are difficult to apply to three-dimensional stress fields. The most common criteria include fracture mechanics, characteristic distance and failure surfaces as defined by polynomial functions of stress tensors. A brief review of these follows to illustrate their limitations. This is followed by a description of the size effect theory that was used for the current study.

Fracture mechanics is typically used to predict the propagation of a single crack in a uniform stress field, although mixed mode criteria for combined tension perpendicular-to-grain and shear stresses have been developed. Unfortunately, the fracture toughness constants for mixed mode fracture are difficult to predict accurately for wood [12]. A single-bolt connection model using fracture mechanics was proposed for wood connections loaded perpendicular-to-grain with uniform stresses throughout the member thickness [13], however, this model was limited in application. In other cases where fracture mechanics was used for connection modelling, researchers have had to introduce fictitious stresses to predict failure [14].

Researchers have successfully applied the characteristic distance concept to multiple-bolt connections in non-wood composites [15–18]. In simple terms, the characteristic distance is a length of material that must be subjected to critical stresses prior to total failure. Thus, once some part of the material has reached critical failure stresses, the analysis is continued until this critical stress is reached all along a pre-selected path. The path and its length are referred to as the characteristic distance. It is likely that this approach has not been used for connections in wood composites because many cases exist where the failure is not entirely brittle and where ductility in the steel bolt affects the overall behaviour.

Another class of criteria are those that use a failure envelope. Detailed reviews of this type of criteria can be found in Refs. [19] and [20]. The simplest criteria are the Maximum Stress and Maximum Strain criteria that assume failure to occur when one of the principal stresses (or strains) exceeds the critical stress (or strain) for that direction. For isotropic materials, the critical value is the same in all directions. While these criteria do not account for stress interactions, they are simple to apply and the critical material strength can normally be determined from straightforward uniaxial tests.

For orthotropic materials, the tensor polynomial Tsai-Wu failure theory [21] can be used to relate normal stresses and shear stresses and their interactions according to

$$f(\sigma_k) = F_i\sigma_i + F_{ij}\sigma_i\sigma_j = 1 \quad \text{where } i,j \text{ and } k = 1,2,3,\ldots,6 \tag{5}$$

Failure occurs when $f(\sigma_k)$ is greater than 1. The polynomial represents a failure surface in stress space. Higher order tensors are typically removed from the polynomial in practice to make the criterion manageable. Differences in tension and compression strengths are accounted for in the parameters F_i and F_{ii}. These functional terms can be determined from straightforward uniaxial strength tests as shown in Ref. [21]. F_{ij} interaction terms, however, are not clearly defined although some researchers have attempted to find a theoretically based equation for these terms [22,23]. The proposed interaction equations for F_{ij} require experiments under various stress combinations and at magnitudes which vary over a range of angles to the axes of orthotropy (off-axis testing) followed by calibration of the equation through curve-fitting. Experiments have been proposed to determine these terms for non-wood composites but they remain difficult to obtain [21,24,25]. For wood composites, it was shown that, for a two-dimensional model, the Tsai-Wu criterion with the interaction terms could be used to predict failure providing that size effects were incorporated in the prediction of failure strengths [26]. Thus, the failure theory produced adequate results with the interaction terms

included. Some researchers have assumed the interaction terms to be zero in their analyses [25] because determining these terms requires a considerable amount of testing even for just one coefficient, as was shown by Clouston in Ref. [26]. While this may be sufficient for two-dimensional analyses, arbitrarily zeroing the interaction terms of the failure tensor should be avoided in three-dimensional analyses [27] and, in particular, for wood [28]. A review of research on failure prediction of bolted connections suggested that considerable development of failure criteria is still required for wood [28].

To this point, deterministic failure theories have been discussed. Probabilistic failure prediction can be incorporated into some of these models to account for variability in wood composites. The Weibull weakest link theory has been used, in the past, to predict the strength of wood members and connections in wood [29–31] and is now generally accepted for wood. The Weibull theory and the Maximum Stress theory were chosen for the current study for the following beneficial reasons: (1) it applies to non-uniform stress fields and amplifies stress concentrations using the *shape* parameter (defined shortly); (2) failure can be predicted for a given probability; (3) material variability is captured and (4) while this approach is continuum based, the amplification of highly stressed regions enables the analyst to isolate the location of critical stresses and the mode(s) of failure.

The Weibull weakest link theory [32] postulates that for brittle materials, larger specimens are more likely to fail at lower stresses due to the increased probability of a flaw in that larger specimen volume. The probability of brittle failure, F_V, based on a two-parameter Weibull distribution is a function of the stress distribution over the volume of material

$$F_V = 1 - e^{-\frac{1}{V^*}\int_V \left(\frac{\sigma}{m}\right)^k dV} \tag{6}$$

where V^* is a reference volume k is the shape parameter, m is the scale parameter associated with the reference volume, and σ is the stress (tension or shear, in any given direction or plane, respectively). The reference stress is based on experimental results. The failure stress for a given probability of failure, p, is

$$\sigma^* = m[-\ln(1-p)]^{1/k} \tag{7}$$

It can be shown that failure occurs when the reference stress, σ^*, occurring over volume V^*, satisfies the following inequality which relates a complex state of stress over an arbitrary volume to the reference stress

$$\int_V \sigma^k \, dV > \sigma^{*k} V^* \tag{8}$$

This form is similar to the Maximum Stress theory where each stress is treated individually and stress interactions are assumed to have little or no effect. A user-programmable subroutine was written with the following algorithm to evaluate Eq. (8) at each load-step in the finite element analysis post-processor to determine when or if failure occurred due to each of the three normal tension stresses and each of the three shear stresses. The volume integral, I

$$I = \int_V \sigma^k \, dV \tag{9}$$

must be evaluated for each three-dimensional solid element using Gaussian integration. It can be shown that

$$I = \int_{-1}^{1}\int_{-1}^{1}\int_{-1}^{1} \sigma^k |J| \, d\xi \, d\eta \, d\zeta \tag{10}$$

where $[J]$ is the Jacobian in terms of local element coordinates (ξ, η, ζ). The determinant of $[J]$ is equal to the volume of the element in global co-ordinates and is calculated from the nodal co-ordinates and the derivatives of the element shape functions. Gaussian integration was used to evaluate Eq. (10).

The integral (10) is determined for each element and then summed for all elements to give the volume integral over the entire model geometry in global co-ordinates. The operation is repeated for each stress component with its corresponding k. Accuracy is dependent on the number of integration points.

7. Shear block model

The notched shear block is commonly used to determine shear strength of wood. To test the new material model, a three-dimensional finite element model of a shear block was developed and the results were compared with results from laboratory tests. Model geometry and boundary conditions for a single shear block are shown in Fig. 5. Eight-noded, three-dimensional quadrilateral isoparametric brick elements were used for the wood and steel platens. These elements have three displacement degrees-of-freedom at

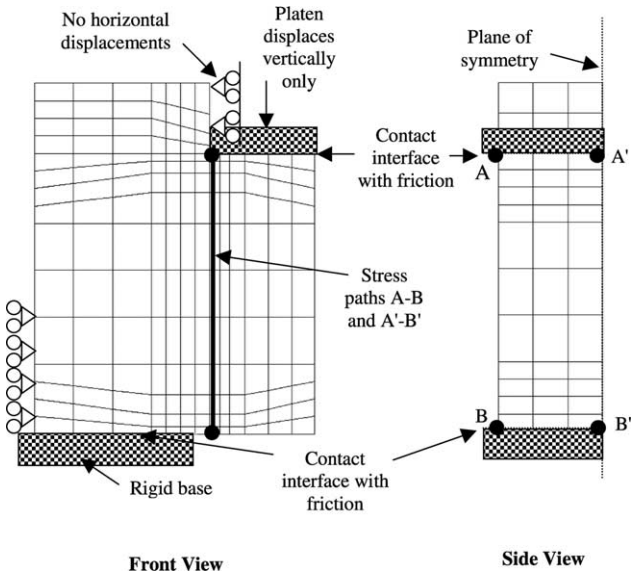

Fig. 5. Shear block finite element model geometry.

each node: UX, UY and UZ. Surface-to-point contact elements were used on interfaces. Planes of symmetry were modelled by setting the relevant displacements to zero on the plane. A typical shear block model had roughly 500 solid elements plus the contact interface elements. A higher mesh density was used in regions of stress concentrations. The steel test frame was simulated using rigid brick elements for the base and loading platen. The base was restricted from moving in each of the three degrees-of-freedom, whereas the loading platen was only allowed to move in the direction of loading, as shown in Fig. 5. The load was applied by displacing the platen. Rollers were placed on the backside of the specimen to simulate the supporting back plate, as indicated in Fig. 5. Only half of the actual shear block was modelled due to symmetry of the specimen. Surface-to-point contact elements were used between the steel frame and the wood specimen to allow gaps to form between the steel and the wood block due to block rotation.

8. Bolted connection tests and modeling

The single-bolt connection test set-up is shown in Fig. 6(a). End and edge distances were chosen to ensure that both brittle and ductile behaviour could be observed. Table 2 lists the typical bolt diameter, member geometry and direction of loading for each panel type.

All bolted connections, regardless of the material, will develop an uneven three-dimensional stress field dependent on the connection geometry and material properties of the members and the connectors. In non-wood composites, the member is relatively thin compared to the bolt resulting in relatively uniform stresses throughout the member thickness; however, in wood composites, the member is much thicker. As a result, bolted connections in wood composites typically exhibit ductility prior to failure: large, permanent deformations of wood cells occur in compression along with yielding of the steel bolt in bending. When a wood member is relatively thin, or end and edge distances are relatively small, brittle failure is observed.

The geometry of the three-dimensional finite element model for the connection was based on a previous model [33], and is shown in Fig. 6(b). The same brick elements were used again in the bolted connection model for the steel bolt and the wood member. Roughly 600 elements were used for the wood member and 500 for the bolt. A contact interface was placed between the bolt and wood. One-quarter of the geometry was modeled by setting displacements to zero on planes of symmetry. The geometry of the model could be modified for changes in end distance, edge distance, member thickness, bolt diameter, hole clearance and support location. To isolate the behaviour of the connector and the highly stressed zone in the wood member, no side members were included in the model. The material model described above was used for each of the five panel types. Panel types C, D and E were simulated by creating a stack of layers with type A and/or B properties.

9. Results: shear blocks

Example load–displacement results are shown in Fig. 3. Since the shear strengths in LSL were unknown, the integral

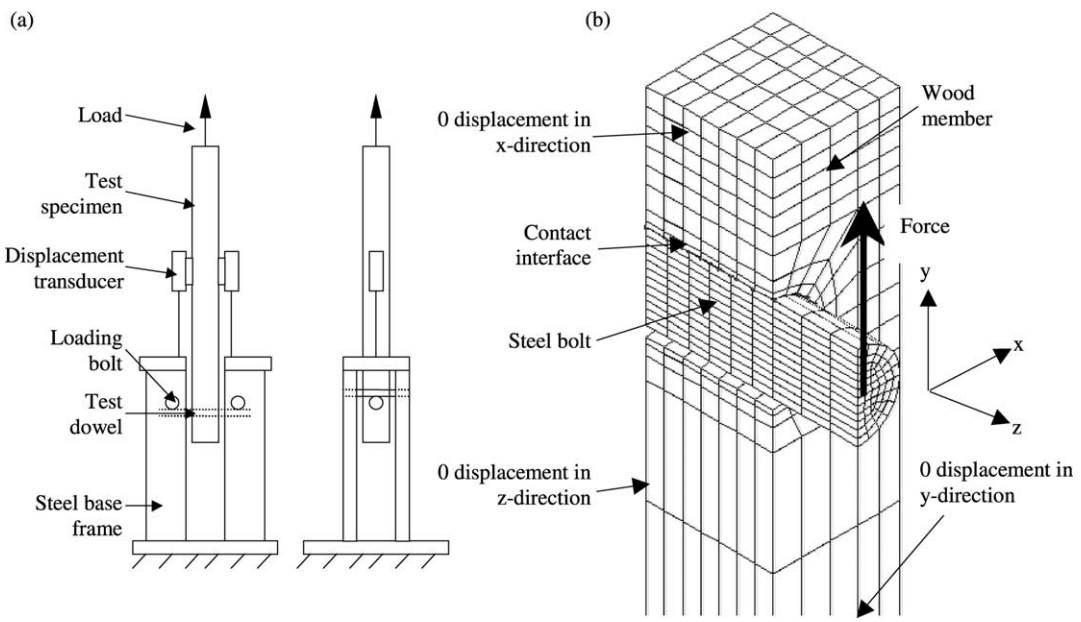

Fig. 6. (a) Connection test set-up (based on Ref. [33]) shown upside-down. (b) Finite element model geometry. Wood properties set parallel-to *Y*-direction, *X*-direction or 45° between, for loading parallel-to, perpendicular-to and at 45°-to-grain, respectively. Properties can be entered for material layers.

Table 2
Single-dowel connection geometry, experimental results and predicted results

Type	*d* (mm)	*e*/*d*	edge/*d*	*l*/*d*	Ultimate load (kN)		Ultimate disp. (mm)		Failure Mode	
					Exp.	Pred.	Exp.	Pred.	Exp.	Pred.
A-Pa	9.5	2	1.5	4	8.0	6.4	2.8	1.3	B	Z
A-Pa	9.5	3	1.5	4	>11.1	>7.3	>7.1	>2.5	D	D
A-Pa	9.5	4	1	4	>10.7	>7.3	>5.8	>2.5	D	D
A-Pa	9.5	4	1.5	4	>10.4	>7.3	>9.9	>2.5	D	D
A-Pa	13	2	1.5	3	12.0	12.2	2.0	1.0	B	Z
A-Pa	13	3	1	3	>19.0	>13.3	>8.4	>1.8	D	D
A-Pa	13	4	1.5	3	>19.4	>13.3	>6.6	>1.8	D	D
A-Pa	19	2	1.5	2	19.8	16.6	1.3	1.0	B	X/Z
A-Pa	19	3	1.5	2	33.0	23.6	2.3	1.5	B	Z
A-Pa	19	4	1	2	>27.5	17.1	>1.5	1.0	NA	Z
A-Pa	19	4	1.5	2	>32.3	26.2	>2.8	1.5	NA	Z
A-Pe	9.5	2	3	4	6.3	5.0	2.0	1.3	B	X
A-Pe	9.5	4	3	4	7.0	5.1	3.3	1.3	B	X
A-Pe	19	2	3	2	15.5	7.5	2.3	1.0	B	X
A-Pe	19	4	3	2	15.2	7.7	2.0	1.0	B	X
A-AN	9.5	2	3	4	8.6	6.4	3.3	1.8	B	X
A-AN	9.5	4	3	4	>10.7	>6.5	>9.9	>1.8	D	D
A-AN	19	2	3	2	18.1	9.1	1.8	0.8	B	X
A-AN	19	4	3	2	27.3	14.8	6.1	1.0	B	X
B-Pa	9.5	2	1.5	4	9.8	6.1	6.1	1.5	B/D	Z
B-Pa	9.5	3	1.5	4	>10.1	>6.2	>9.4	>1.5	D	D
B-Pa	9.5	4	1	4	5.8	5.3	1.0	1.0	B	Z
B-Pa	9.5	4	1.5	4	>10.0	6.2	>8.4	1.8	D	Z
B-Pa	13	2	1.5	3	14.3	11.1	3.6	1.0	B	Z
B-Pa	13	3	1	3	>17.9	12.0	>8.1	1.3	B/D	Z
B-Pa	13	4	1.5	3	>17.0	12.0	>6.9	1.3	D	Z
B-Pa	19	2	1.5	2	24.4	16.3	6.1	1.0	B	Z
B-Pa	19	3	1.5	2	31.4	17.4	4.3	1.3	B	Z
B-Pa	19	4	1	2	14.9	10.3	1.3	0.8	B	Z
B-Pa	19	4	1.5	2	30.9	17.4	6.4	1.3	B	Z
C-Pa	9.5	2	1.5	4	8.7	7.2	5.3	2.8	B/D	Z, 0°
C-Pa	9.5	3	1.5	4	>10.2	>7.0	>7.6	>2.5	D	D
C-Pa	9.5	4	1	4	9.6	>7.1	6.6	>2.5	B/D	D
C-Pa	9.5	4	1.5	4	>11.0	>7.0	>9.9	>2.5	D	D
C-Pa	13	2	1.5	3	15.6	12.2	5.1	1.0	B	Z, 0°
C-Pa	13	4	1.5	3	>20.4	>13.6	>11.4	>1.8	D	D
C-Pa	19	2	1.5	2	22.6	18.1	2.0	1.0	B	Z, 0°
C-Pa	19	3	1.5	2	32.8	23.0	5.3	1.0	B	Z, 0°, R
C-Pa	19	4	1	2	30.0	14.7	2.3	0.8	B	Z, R
C-Pa	19	4	1.5	2	>35.8	>24.4	8.4	1.3	B/D	Z, 0°
C-Pe	9.5	2	3	4	8.8	6.0	5.1	1.5	B	Z, 0°
C-Pe	9.5	4	3	4	>11.0	6.1	>13.2	1.8	B/D	Z, 0°
D-Pa	9.5	2	1.5	4	9.4	6.4	5.8	1.3	B	Z, R
D-Pa	9.5	3	1.5	4	>10.7	>5.5	>9.9	>1.0	D	D
D-Pa	9.5	4	1	4	8.2	5.5	3.6	1.0	D	Z, R
D-Pa	9.5	4	1.5	4	>10.7	>6.3	>11.9	>1.8	D	D
D-Pa	13	2	1.5	3	13.8	11.8	4.1	1.0	B	Z, R
D-Pa	13	4	1.5	3	>20.6	12.6	>11.7	1.3	B/D	Z, R
D-Pa	19	2	1.5	2	27.0	17.8	2.0	1.0	B	Z, R
D-Pa	19	3	1.5	2	34.9	20.6	5.6	1.0	B/D	Z, R
D-Pa	19	4	1	2	24.7	12.5	2.0	0.8	B	Z, R
D-Pa	19	4	1.5	2	32.6	20.7	7.1	1.0	B	Z, R
D-Pe	9.5	2	3	4	>10.4	>6.0	>9.1	>1.3	D	D
D-Pe	9.5	4	3	4	>11.0	>6.2	>13.7	>1.3	D	D
E-Pa	9.5	2	1.5	4	8.6	6.5	3.3	1.5	B	Z, 0°
E-Pa	9.5	3	1.5	4	>10.4	>7.3	>10.9	>2.5	B/D	D
E-Pa	9.5	4	1	4	9.7	6.5	5.1	1.5	B	Z, +45°
E-Pa	9.5	4	1.5	4	>11.3	>7.3	>10.7	>2.5	D	D
E-Pa	13	2	1.5	3	13.6	13.0	3.6	1.8	B	Z, 0°

(*continued on next page*)

Table 2 *(continued)*

Type	*d* (mm)	*e*/*d*	edge/*d*	*l*/*d*	Ultimate load (kN)		Ultimate disp. (mm)		Failure Mode	
					Exp.	Pred.	Exp.	Pred.	Exp.	Pred.
E-Pa	13	4	1.5	3	>21.5	>12.8	>11.2	>1.5	D	D
E-Pa	19	2	1.5	2	24.4	19.8	2.0	1.3	B	Z, 0°
E-Pa	19	3	1.5	2	37.8	23.1	6.9	1.5	B	XY, +45°
E-Pa	19	4	1	2	24.5	15.0	1.8	1.0	B	Z, 0, ±45°
E-Pa	19	4	1.5	2	>37.1	22.1	>7.9	1.3	D	XY, +45°
E-Pe	9.5	2	3	4	>10.0	5.1	>8.9	1.0	B/D	X, 0°
E-Pe	9.5	4	3	4	>10.9	>5.6	>10.7	>1.8	B/D	D

NA, no failure achieved to due grip limitations; X, Z, XY indicate tension failures in *X* and *Z*-directions and shear failure in the *XY*-plane, respectively; 'B' indicates brittle fracture occurred; D indicates no fracture occurred and behaviour was ductile; R, 0 and ±45° indicate layer in which failure was found to occur (random or oriented at 0 or ±45°, respectively).

of Eq. (8) was evaluated to back-calculate the reference shear stress for a unit volume at the end of the analysis. After detailed analysis, failure of these specimens was found to be governed by the development of tension stresses perpendicular to the panel thickness, not shear stresses. The model was used to prove that a stress concentration of roughly two (2) at the notch leads to premature failure of the specimens [3].

10. Results: bolted connections

Average results of laboratory single-bolt connection tests are listed in Table 2 along with the predicted model results for $p = 0.5$. Two sample load–displacement curves are shown in Fig. 7. These plots are shown here to illustrate the difference in ductility between specimen groups. Both specimen groups followed a very similar load–displacement path, however, specimens with small end distance, $2d$, failed earlier than those with $4d$ end distance. Model results are superimposed on the experimental curves shown in Fig. 7. The predicted curves end at the lesser of: (a) the point of predicted failure based on $p = 0.5$ (i.e. average values) or (b) 2.5 mm (the point at which the analysis was stopped).

Ultimate loads were always predicted conservatively to be within 50–84% of the experimental averages for all specimen groups and loading orientations. The reason for the conservative estimates is that failure of the entire connection was assumed to occur at the first instance that the governing stresses (tension or shear) reached capacity. Thus, if delamination (i.e. tension in the *Z*-direction) failure was predicted to start in the specimen at a particular load, then the analysis was stopped—in reality, the specimen would continue to carry more load until it would either fail under the initial failure condition, or under an entirely different mode that could become critical at a later stage.

Ductile behaviour was predicted to occur when the load–displacement curve exhibited non-linearity and when the failure criterion was not satisfied up to the 2.5 mm displacement level. The mode of failure was predicted near to the observations from experiments as indicated in Table 2. The model was found to be well behaved for predicting the failure modes in all loading orientations, as indicated in Table 2. In addition, the layer in which failure occurs is predicted for multiple-layer panels C, D and E. Shear stress concentrations in Fig. 8 show the distinct differences between fully oriented specimens and eight-layer type E specimens. Type A has more or less uniform stress distribution throughout its thickness, whereas type E has stress concentrations at the interfaces of the layers.

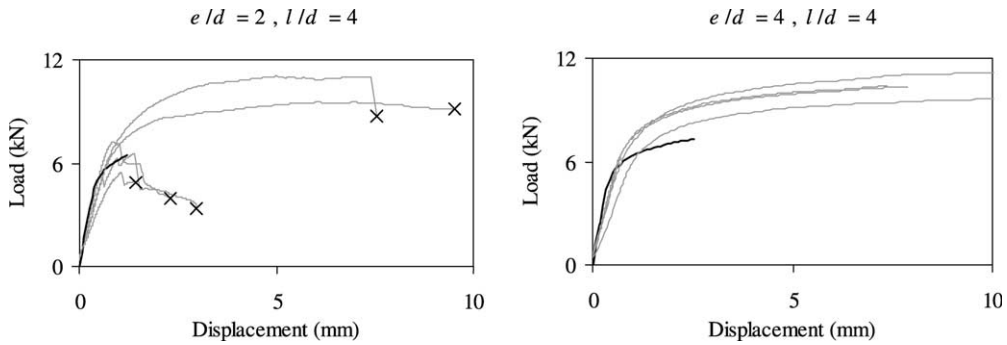

Fig. 7. Load–displacement curves for fully oriented type 'A' LSL panels loaded parallel-to-grain. 'X' indicates point of failure due to splitting in specimens with $e/d = 2$. Specimens with $e/d = 4$ exhibited ductile behaviour only. Analytical predictions are shown as bold curves.

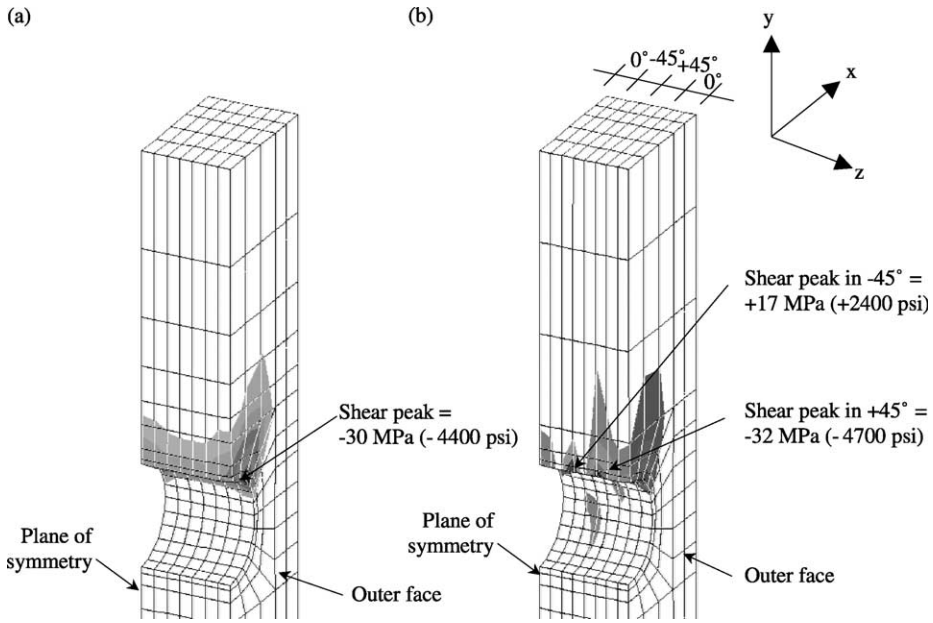

Fig. 8. Stress contours of shear stress, σ_{xy}, in LSL loaded parallel-to-grain. (a) Type 'A' material and (b) type 'E' material at failure load, with $e/d = 4$, edge distance $1.5d$ for specimen with 19 mm dowel, $l/d = 2$.

11. Conclusion

The proposed new material model for wood composites was shown to perform well for the two sample cases as discussed. For shear blocks, the model was used to determine shear constants and to confirm that the notch results in a stress concentration that leads to under-estimated strength predictions. For bolted connections, the material model was found to predict load–displacement, ultimate strength and mode of failure with reasonable accuracy for many variables including wood species, panel lay-up and connection geometry. The model has already been used to make strength and behaviour predictions of multiple-bolt connections [34].

This material model will allow manufacturers to predict the effects of changing orientation within their products and enable them to optimize their products through control of strand orientation. The model is capable of determining the effect of changes in material properties as may occur when other species of trees are considered for raw materials. The single-bolt connection model is particularly significant as it explains many of the observed phenomena from experimental studies with respect to end distance, edge distance and modes of failure.

Acknowledgements

Financial support for this project was provided by the Science Council of British Columbia, Trus Joist Weyerhaeuser Limited and Forest Renewal British Columbia.

References

[1] Moses DM, Prion HGL, Li H, Boehner W. Composite behaviour of laminated strand lumber. Wood Sci Technol 2003;37:59–77.
[2] Moses DM, Prion HGL. Anisotropic plasticity and the notched wood shear block. Prod J 2002;52(6):43–54.
[3] ASTM D1037, Standard test methods of evaluating the properties of wood-base fiber and particle panel materials. Pennsylvania: American Society for Testing and Materials; 1996.
[4] ASTM D143, Standard methods of testing small clear specimens of timber. Pennsylvania: American Society for Testing and Materials; 1996.
[5] Chen WH, Lee S, Yeh JT. Three-dimensional contact stress analysis of a composite laminate with bolted joint. Comput Struct 1995;30(3): 287–97.
[6] Camanho PP, Matthews FL. Stress analysis and strength prediction of mechanically fastened joints in FRP: a review. Composites Part A 1997;28A:529–47.
[7] ANSYS, ANSYS v.5.3. Houston, Pennsylvania: Swanson Analysis Systems Inc.; 1996.
[8] Vaziri R, Olson MD, Anderson DL. A plasticity-based constitutive model for fibre-reinforced composite laminates. J Compos Mater 1991;(25):512–35.
[9] Hill R. A theory of the yielding and plastic flow of anisotropic metals. Proc R Soc Ser A 1947;193:281–97.
[10] Shih CF, Lee D. Further developments in anisotropic plasticity. Trans ASME, J Engng Mater Technol July 1978;100:294–302.
[11] Valliappan S, Boonlaulohr P, Lee IK. Non-linear analysis for anisotropic materials. Int J Numer Meth Engng 1976;10:597–606.
[12] Fonselius M, Riipola K. Determination of fracture toughness for wood. J Struct Engng ASCE 1992;118(7):1727–40.
[13] Smith I, Hu LJ. Fracture analysis of bolted timber connections. In: ASCE Structures Congress XII: Proceedings of papers presented at the structures congress 1994, Atlanta, GA; April 1994. p. 912–7.
[14] Jorissen A. Double shear timber connections with dowel type fasteners. PhD Thesis. Delft University, Netherlands; 1998
[15] Hyer MW, Chastain PA. Effect of bolt load proportioning on the capacity of multiple-bolt composite joints. J Aircraft 1988;25(2):184–9.

[16] Cohen D, Hyer MW, Shuart MJ, Griffin OH, Prasad C, Yalamanchili SR. Failure criterion for thick multi-fastener graphite-epoxy composite joints. J Compos Technol Res 1995;17(3):237–48.
[17] Eriksson I, Backlund J, Moller P. Design of multiple-row bolted composite joints under general in-plane loading. Compos Engng 1995;5(8):1051–68.
[18] Arnold WS, Marshall IH, Wood J. Optimum design considerations for mechanically fastened composite joints. Compos Struct 1990; 16(1–3):85–101.
[19] Rowlands RE. Strength (failure) theories and their experimental correlation. In: Sih GC, Skudra AM, editors. Failure mechanics of composites, vol. 3. Amsterdam: North-Holland; 1985. p. 71–125.
[20] Nahas NN. Survey of failure and post-failure theories of laminated fibre-reinforced composites. J Compos Technol Res 1986;8(4):138–53.
[21] Tsai SW, Wu EM. A general theory of strength for anisotropic materials. J Compos Mater 1971;5:58–80.
[22] Cowin SC. On the strength anisotropy of bone and wood. J Appl Mech, ASME Trans 1979;46(4):832–7.
[23] Liu JY. Evaluation of the tensor polynomial strength theory for wood. J Compos Mater 1984;18:216–26.
[24] Wu EM. Optimal experimental measurements of anisotropic failure tensors. J Compos Mater 1972;6:472–89.
[25] Narayanaswami R, Adelman HM. Evaluation of the tensor polynomial and Hoffman strength theories for composite materials. J Compos Mater 1977;11:366–77.
[26] Clouston P. The Tsai-Wu strength theory for Douglas-fir laminated ve-neer. MSc Thesis. University of British Columbia, Vancouver, BC; 1995.
[27] Theocaris PS, Philippidis TP. On the validity of the tensor polynomial failure theory with stress interaction terms omitted. Compos Sci Technol 1990;38/39:181–91.
[28] Patton-Mallory M, Cramer SM, Smith FW, Pellicane PJ. Nonlinear material models for analysis of bolted wood connections. J Struct Engng 1997;123(8):1063–70.
[29] Barrett JD. Effect of size on tension perpendicular-to-grain strength of Douglas fir. Wood Fiber 1974;6(2):126–43.
[30] CSA, Engineering design in wood (limit states design). Standard O86.1-94, Rexdale, Ont. Canadian Standards Association; 1994.
[31] Foschi RO, Longworth J. Analysis and design of griplam nailed connections. J Struct Div, ASCE, ST12 December 1975;101: 2537–55.
[32] Weibull W. A statistical theory of strength of materials. Proceedings of Royal Swedish Institute, Stockholm: Engineering Research No.151; 1939.
[33] Patton-Mallory M. The three-dimensional mechanics and failure of single bolt wood connections. PhD Thesis. Colorado State University, Fort Collins, CO; 1996
[34] Moses DM, Prion HGL. A three-dimensional model for bolted connections in wood. Can J Civ Engng 2003;30:555–67.